SPECIAL ISSUE

3D Printing Technologies for Environmental and Water Applications

ACS Publications
Most Trusted. Most Cited. Most Read.

Search text, DOI, authors, etc.

˅ ABSTRACT

Molecular Response of Dissolved Organic Matter in Aquifer to Landfill Leachate Leakage

Xian-Ge Wang, Wei He, Xian-Jiang Zeng, Xu Cao, Qing-Yu Liu, and Xiao-Song He*

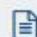📄 Abstract   📄 Full text   📄 PDF

˅ ABSTRACT

Waste-to-Wealth: Unlocking the Potential of Pine Sawdust Biochar for Adsorption of Cobalt(II) and Nickel(II) Ions and Sustainable Elimination of Carbamazepine from Aqueous Solutions

Anna Yukhymchuk, Daria Zhukova, Nataliia Prybora, Nataliya Stolyarchuk, Oleksandr Bondarchuk, Halyna Bodnár Yankovych*, and Inna V. Melnyk*

📄 Abstract   📄 Full text   📄 PDF

˅ ABSTRACT

Waste-to-Wealth: Unlocking the Potential of Pine Sawdust Biochar for Adsorption of Cobalt(II) and Nickel(II) Ions and Sustainable Elimination of Carbamazepine from Aqueous Solutions

Anna Yukhymchuk, Daria Zhukova, Nataliia Prybora, Nataliya Stolyarchuk, Oleksandr Bondarchuk, Halyna Bodnár Yankovych,* and Inna V. Melnyk*

Cite This: ACS EST Water 2024, 4, 3943−3955

Read Online

ACCESS | ⠿ Metrics & More | 🔖 Article Recommendations | SI Supporting Information
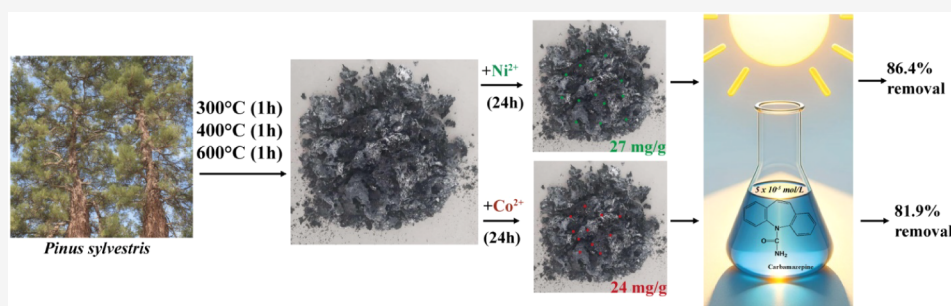
ABSTRACT: Sustainable waste management is the recycling, reusing, and recovery of wastes from natural sources. This research studied the conversion of *Pinus sylvestris* residues into sustainable biochars with improved properties for the adsorption of Co(II) and Ni(II) with further usage of spent biochars in the removal of carbamazepine. The biochars possessed high surface areas and abundant chemical composition with equilibrium adsorption capacities of 0.38 mmol/g for Co(II) and 0.48 mmol/g for Ni(II), forming cobalt phosphate and nickel hydroxide on the biochar surface. The laden biochars efficiently removed carbamazepine through adsorption and under UV light, following a first-order kinetic model with rate constants ranging from 0.0031 to 0.0042 min^{-1} and achieving an efficiency of over 80%. The complex interaction mechanisms were responsible for the reduction of the carbamazepine concentration in the studied systems. This research demonstrates that waste wood raw materials can be used as synergistic multifunctional materials.

KEYWORDS: *sustainable material, pine waste biochar, cobalt(II) ions, nickel(II) ions, UV treatment, carbamazepine removal*

■ INTRODUCTION

The Eurostat statistics on waste for the year 2020 highlight significant aspects of waste generation and treatment within the European Union. In 2020, the EU generated approximately 2.135 billion tonnes of waste, averaging around 4.815 kg per capita. A substantial portion of this waste, about 59.1%, underwent recovery processes, including recycling, backfilling, or incineration with energy recovery. Meanwhile, 40.9% of the waste was disposed of through methods such as landfilling and incineration without energy recovery. The statistics emphasize the scale of waste generation in the EU and the substantial efforts toward waste recycling and recovery.[1]

However, general research on waste management and the utilization of waste materials, including pine-related waste, indicates that managing such waste responsibly is crucial for environmental sustainability. For instance, studies on biochar and activated carbon derived from various types of waste, including pine, highlight the potential of these materials in environmental remediation and pollution control. Moreover, broader studies on waste management challenges, including

the research by Carmo et al.[2] on the environmental risks of mining wastes, demonstrate the significance of managing large-scale waste, including forestry and agricultural residues, to prevent environmental degradation. These studies underscore the importance of sustainable waste management practices and the potential of waste materials, including pine, in various environmental applications.

The management of waste from pine, including its utilization and potential environmental impacts, is a topic explored in various research studies. Vieira et al.[3] examined the use of pine bark and wood chips mixed with compost for biofiltration in a municipal waste management plant. This study highlights the

potential of pine-derived materials in odor control and waste treatment processes. Yaman[4] encompasses research on the pyrolysis of various types of biomass, including urban and industrial waste, aimed at producing fuel and chemical raw materials, analyzing the characteristics of pyrolysis products and methods for their improvement for economically and environmentally acceptable use. This study underscores the versatility of pine waste in sustainable agriculture and energy recovery. Also, one of the biomass applications discussed biomass gasification as an advanced technology[5] for replacing fossil fuels, reviewing various gasifiers and methods, including supercritical water gasification, and outlines its potential in producing valuable products such as syngas, biofuels, and power, contributing to the reduction of global warming and ecological imbalance. The development and evaluation of an ash pretreatment process to enhance the sorption of 2,4-dichlorophenoxyacetic acid (2,4-D) and sulfamethoxazole (SMX) by pine and biosolids-based biochars were conducted, making them competitive with commercial powdered activated carbon (PAC) and applicable in low-cost water treatment scenarios, including stormwater and wastewater treatment, with a significant improvement in sorption performance.[6] Furthermore, Musapatika et al.[7] evaluated pine sawdust as an adsorbent in treating wastewater containing cobalt ions and for environmental protection. In addition, Rashad et al.[8] demonstrate that biochar derived from pinewood sawdust is an effective and economically feasible biosorbent for removing polycyclic aromatic hydrocarbons from wastewater, with different activation methods enhancing its adsorption efficacy. Another study reveals that biochar produced from pine sawdust at various pyrolysis temperatures is a cost-effective alternative to activated carbon for removing p-nitrophenol from water, with its adsorption efficacy influenced by the biochar's physicochemical properties, preparation temperature, and environmental conditions.[9] Besides sawdust, the use of biochar from pine needles[10] has also demonstrated significant potential in adsorbing caffeine from water, with its efficiency influenced by temperature, showing that this process is endothermic and entropy-driven. Kim et al.[11] reveal that pine sawdust biochar, especially when modified with Mg/Al layered double hydroxides, significantly enhances the adsorption capacity for azo dyes such as Methyl Orange and Sunset Yellow FCF, with a notable improvement in adsorption mechanisms and excellent reusability, despite having a lower specific surface area compared to unmodified biochar. As well the review emphasizes the use of waste materials, such as pine sawdust, as cost-effective adsorbents for water purification, reducing the cost of water treatment technologies and contributing to environmental protection.[12] Overall, these studies reveal the diverse applications of pine waste in environmental management, energy production, and agriculture, highlighting its potential as a valuable resource in sustainable practices.

In the context of escalating environmental concerns, particularly regarding water pollution, the degradation of persistent pharmaceutical contaminants has garnered substantial attention.[13] Among these, carbamazepine (CBZ), a widely used anticonvulsant and mood-stabilizing drug, poses a notable challenge, while a recommended therapeutic dose in plasma is established within a 4−12 μg/L concentration range.[14,15] Its recalcitrant nature in environmental matrices underscores the necessity for innovative and effective remediation strategies.[16] Carbamazepine is not expected to undergo any significant degradation in typical municipal wastewater treatment plants.[17] The intensive research on carbamazepine removal from sewage wastewater has demonstrated that this drug is only slightly eliminated from the wastewater during the treatment (if any, then less than 10%). Carbamazepine permissible level in groundwater is estimated at 0.5 μg/L as a general standard for all pharmaceuticals; however, Scientific Committee on Health, Environmental and Emerging Risks (SCHEER) reveals some concerns that this value could not be protective enough for groundwater ecosystem.[18]

Carbamazepine can be found in different types of water wastes, especially household wastewater, in a variety of ranges—from 0.035 to 6.3 μg/L.[19] For instance, the studies of Canadian water resources demonstrated that the highest concentration of carbamazepine in surface water was measured approximately at 1 μg/L and in municipal sewage discharges at 2.3 μg/L.[20,21]

The carbamazepine-contaminated liquid wastes are usually discharged to local municipal wastewater treatment plants. However, the treatment procedures frequently are not as effective as expected, which causes further migration of untreated carbamazepine molecules or their metabolites into important water sources. Therefore, wastewater require additional purification technologies that would be able to effectively eliminate the pollutant. A promising avenue in this pursuit is the exploration of photocatalytic degradation techniques, which have emerged as a potent tool for tackling such persistent organic pollutants.[22] Carbamazepine is a common pharmaceutical contaminant posing serious environmental and health threats.[23] The study of its photocatalytic degradation is crucial for addressing these concerns within the combination of ecofriendliness and performance, especially in the removal of organic pollutants.

The photocatalytic elimination of carbamazepine has been tested in a variety of concentration ranges, which depend on the target wastewater source and its physicochemical characteristics, available analytical tools, and performance of the photocatalyst. Thus, the authors described the decomposition of carbamazepine at a concentration of 20 mg/L under visible light in the presence of doped ferrites, achieving a removal efficiency of 94.3%.[24] The elimination of carbamazepine with $BiPO_4$ synthesized via a hydrothermal method from simulated wastewater (C_{CBZ} = 5 mg/L) demonstrated a 72.4% concentration decrease after 60 min of light exposure.[25] Comparable results were obtained by the authors,[26] who achieved a 71.41% reduction of C_{CBZ} = 10 mg/L using UVA light-driven g-C_3N_4/TiO_2 composite, with the mineralization yield of ~30% from initial carbamazepine molecules. Very impressive results were detailed in,[22] where researchers successfully degraded 5 mg/L of carbamazepine using Ag_3PO_4/GO under visible light, employing ●OH and O_2^-● as the reactive oxygen species.

While the specific studies focusing on biochar derived from pine and adsorbed nickel or cobalt ions are limited, related research highlights the importance of exploring innovative photocatalytic materials and methods for degrading pollutants such as carbamazepine. For instance, Gao et al.[27] investigated the effects of inorganic ions on the photocatalytic degradation of CBZ, emphasizing the complex interactions in such processes. Additionally, the potential of various photocatalysts in environmental remediation was studied on the photocatalytic degradation of CBZ using bismuth oxychlorides

underlines.[28] Further research in this area, particularly focusing on biochar-based photocatalysts with nickel or cobalt ions, would contribute significantly to the field of environmental pollution control and sustainable water treatment technologies.[29−32] The use of biochar derived from pine as a base for photocatalysts is a sustainable and environmentally friendly approach. It utilizes renewable resources and offers an effective way to treat water contaminated with pharmaceuticals such as CBZ. The modification of these photocatalysts with adsorbed nickel or cobalt ions could potentially enhance their effectiveness, leading to more efficient degradation processes. Nickel and cobalt ions are known for their catalytic properties, including their ability to facilitate electron transfer processes, which are crucial in photocatalysis. By adsorbing these ions onto the biochar surface, it is hypothesized that the resulting photocatalysts can offer improved efficiency in degrading CBZ under light irradiation. This approach not only shows potential for mitigating the environmental persistence of carbamazepine but also provides a sustainable attempt to reduce the carbamazepine concentration to the permissible level of pharmaceuticals in modeled aqueous systems.

■ EXPERIMENTAL SECTION

Synthetic Approaches. To prepare sorption materials, this study utilized plant waste, specifically sawdust from Scots pine (*Pinus sylvestris*), which is a predominant forest-forming species in Europe and Asia. The chemical composition of pine wood may vary based on various factors such as the age of the trees, the type of soil they grow in, and abiotic environmental factors.

The collected pine sawdust was then dried for 2 h at 105 °C to eliminate physically bound water with a mass loss of approximately 37%. Building on the analysis of literature data, we adapted established methods for charring plant material,[33−35] which were applied to produce sorbents to investigate their physicochemical and sorption characteristics. The resulting dry biomass was subjected to carbonization by pyrolysis (Figure 1).
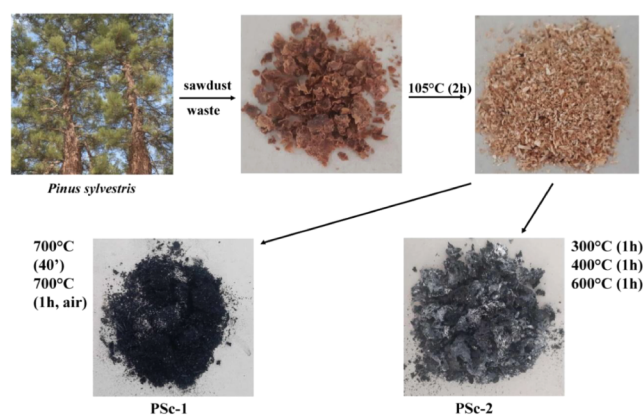

Figure 1. Synthetic ways of obtaining biochar samples from *Pinus sylvestris* waste.

PSc-1 Sample. The charring of the material was conducted at a temperature of 700 °C in a muffle furnace SNOL-1,6.2,5.1/12-I2 in two stages: initially, to prevent ignition, crucibles with lids were utilized, and the samples were maintained within them for 40 min; subsequently, they were opened and calcined for an additional hour. The sample

exhibited a yield of 9.1% when calculated from the wet raw material and 14.5% from the dry raw material.

PSc-2 Sample. The charring of the biomaterial was performed in three distinct modes in open crucibles. The starting temperature was 300 °C, which was then raised to 450 °C, and finally, the maximum temperature reached was 600 °C. The material was held at each temperature for 1 h.

The resulting samples were cooled in a desiccator, homogenized, and transferred to jars with sealed lids for storage. The yield of the sample was 8.0% based on the wet raw material and 12.9% based on the dry raw material.

Preparation of **PScw-1** and **PScw-2** samples: Considering the high mineral content in the prepared biochars, which could potentially skew the analysis of their adsorptive and photocatalytic features, the materials underwent extensive washing with copious amounts of deionized water, accompanied by constant monitoring of the pH levels in the filtrates. The cleansing procedure was considered finished once the pH levels in the filtrates were stabilized for a minimum of two consecutive cycles. The mass loss after water washing was 0.8% for sample **PSc-1** and 0.65% for sample **PSc-2**.

Methods and Techniques. The study analyzed the number of functional groups on the sample surfaces and measured total acidity and basicity using the Böhm titration method.[36]

The photocatalytic tests were carried out in a custom-built photocatalytic reactor operating in batch mode at room temperature.[37] (See Supporting Information).

■ RESULTS AND DISCUSSION

Structure and Texture of the Biochar Samples. The pyrolysis of pine residues at 700 °C, conducted with and without oxygen, affects the final biochar properties based on the intrinsic characteristics of the biomass and desired outcomes. Pyrolyzing at this temperature without oxygen access produces syngas, while a low-oxygen environment promotes biochar formation with high carbon content and porosity. Meanwhile, the stepwise pyrolysis for **PSc-2** biochar at 300 °C, 400 °C, and 600 °C optimizes the decomposition of hemicellulose, cellulose, and lignin respectively, enhancing the biochar's structural properties and suitability for specific applications. This methodical temperature increase allows for controlled thermal decomposition, maximizing the yield and effectiveness of the resulting biochar.[38] (See Supporting Information.)

The morphology of the samples was studied by scanning and transmission microscopy (Figure 2). The SEM image in Figure 2a shows the biochar, revealing a fibrous structure with visible pores and cavities along the length of the biochar. The surface appears rough with several elongated, tube-like formations, indicative of the structural remnants of the pine's vascular system. The TEM image of the **PSc-1** sample allows for observing the agglomerated particulate nature of the biochar. The particles appear as densely packed, irregularly shaped clusters with a broad size distribution, highlighting the porous and fragmented texture characteristic of biochar produced from pine (Figure 2b).

The SEM image of biochar **PSc-2** obtained at another temperature regime further illustrates the heterogeneous and porous surface, featuring large voids and a rugged texture that suggests a high surface area, which is beneficial for adsorption processes (Figure 2c). The TEM image of the **PSc-2** sample demonstrates that the particles form loosely bound clusters
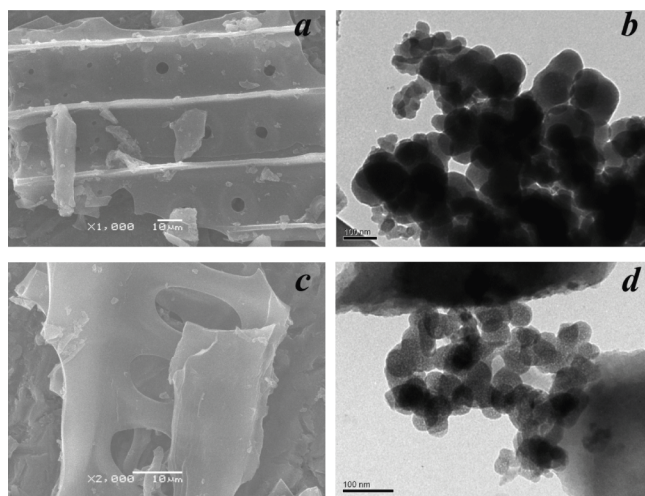
Figure 2. SEM and TEM images of the **PSc-1** sample (a and b) and the **PSc-2** sample (c and d), respectively.

with considerable porosity between them. The morphology suggests that these structures could offer advantageous properties due to their extensive surface area and porosity (Figure 2d).

Overall, the biochar samples derived from pine exhibit a complex morphology that includes both fibrous structures and particulate clusters, which are characterized by a high degree of porosity and surface irregularities. These features are indicative of the material's potential for applications requiring high surface area and adsorption capacity, such as environmental remediation and catalysis.

Thermogravimetric analysis (Figure S1) revealed that synthesized biochars showed initial moisture-related weight loss below 100 °C, remained stable up to 300 °C, and then underwent significant decomposition, primarily of hemicellulose and cellulose,[39] with total mass losses of 94.5% for **PSc-1** and 96.2% for **PSc-2**.

An interesting observation was made based on gas sorption analysis. As shown in Figure 3, both biochars demonstrated large values of specific surface area in comparison to other nonactivated biochars:[40] 347 m^2/g for **PScw-1** and 272 m^2/g for **PScw-2**. The isotherms are characteristic of microporous materials with *Type I* shape with a micropore volume of approximately 0.12 cm^3/g for each material. This feature can be explained by different carbonization procedures of the

PScw-1 and **PScw-2** samples. It is known that the charring temperature affects the textural properties of biochars and is a determinative factor for the values of the specific surface areas.[41] The increase in the carbonization temperature leads to the enhancement of S_{BET}, which was also confirmed for prepared biochars. In summary, the nitrogen adsorption isotherms for the biochar samples **PScw-1** and **PScw-2** reveal significant porosity with a mix of micro- and mesopores, making them suitable for applications requiring high surface area and efficient adsorption properties.

X-ray diffraction patterns for biochar samples **PSc-1** and **PSc-2** and their washed counterparts, **PScw-1** and **PScw-2**, presented in Figure S2, show a broad peak around 20−30 degrees (2θ), indicative of the amorphous carbon structures typical in biochar, which lack long-range order. At approximately 29.5 degrees (2θ), peaks often correspond to calcium carbonate (CaCO$_3$) in its calcite form, commonly present in biomass and biochar due to the mineral content of the feedstock.[42,43] The washing process, as seen in **PScw-1**, appears to remove some surface impurities or inorganic components, evidenced by slightly lower intensity peaks, potentially increasing the order within the carbon structure. Notably, the peak at around 44 degrees (2θ) corresponds to disordered graphitic carbon, indicative of the stacking of graphene layers, and remains broad in all samples, reflecting the disordered or turbostratic structure of the carbon atoms.[44] The presence of typical carbon structure peaks after carbonization confirms the complete decomposition of raw materials and the development of specific aromatic carbon frameworks.[45]

The elemental compositions of the prepared materials are presented in Table 1. The elemental analysis of the biochar samples shows interesting trends in the changes in nitrogen (N), carbon (C), and hydrogen (H) content depending on the pyrolysis temperature and the effect of water washing. All samples exhibit an increase in carbon content with an increase in pyrolysis temperature (**PSc-1** has more C than does **PSc-2**). This could be associated with a higher degree of carbonization at higher temperatures.[39] Biochars possess a high content of nitrogen, which can be beneficial in adsorption of metal ions.[46,47] Lower pyrolysis temperatures tend to preserve more nitrogen in the biochar, while higher temperatures may lead to greater nitrogen loss due to volatilization of nitrogenous compounds.[48] Washing with water (**PScw-1**) appears to reduce the C,N,H contents compared to unwashed sample **PSc-1**, possibly due to the removal of small and labile organic compounds. In the case of the **PScw-2** sample, the observed
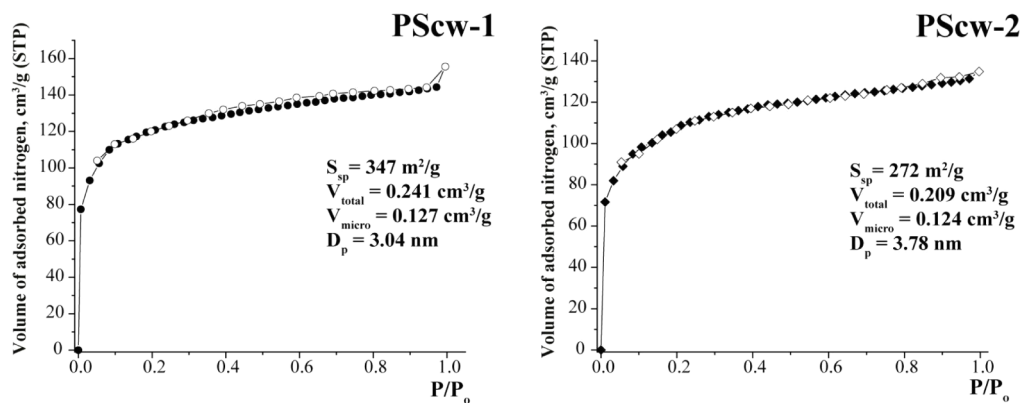

Figure 3. Nitrogen adsorption−desorption isotherms.

Table 1. Composition and Some Sorption Characteristics of the Obtained Biochars

sample	C, mass %	N, mass %	H, mass %	C/H ratio	C/N ratio	C_N, mmol/g	H_2O vapor uptake, mg/g	petroleum ether vapor uptake, mg/g (cm^3/g)
PSc-1	76.92	0.96	3.12	24.7	79.9	0.69	0.103	0.23 (0.348)
PScw-1	76.25	0.85	2.85	26.7	90.1	0.61	0.181	0.136 (0.205)
PSc-2	69.33	0.89	2.99	23.2	77.8	0.63	0.266	0.125 (0.189)
PScw-2	73.26	1.08	2.62	27.9	67.9	0.77	0.292	0.183 (0.277)

increase in the C,N,H contents after washing suggests that leaching of various inorganic salts occurred. This process generally impacted the sample's mass and resulted in the redistribution of elemental masses within the biochar. As well, the ratio of carbon and hydrogen was approximately the same for all samples, which shows a similar graphitization degree of designed biochars.[39]

To study the nature of the surface of the prepared samples, the adsorption of water and petroleum ether vapors was studied under standard conditions (20 °C, 1 atm). It can be concluded that the **PScw-1**, **PSc-2**, and **PScw-2** samples are more hydrophilic than hydrophobic, while the **PSc-1** sample shows the opposite tendency. A possible explanation lies in the data from Table 2, which presents titration results. Both

**Table 2. Data on the Number of Functional Groups Determined by Böhm Titration**

	group concentration, mmol/g	
functional groups	PScw-1	PScw-2
carboxylic	0.06	0.12
lactone	0.55	1.10
phenolic	2.33	2.17
total acidity	2.95	3.40
total basicity	0.98	2.67

washed samples have different types of hydrophilic groups, and the number of surface groups in **PScw-2** is significantly higher. Therefore, the data from vapor adsorption and Böhm titration are in agreement and indicate that the **PScw-2** sample is more chemically functionalized than **PScw-1**, possessing higher total acidity and significantly higher basicity, which may influence its adsorption properties, pH buffering capacity, and utility in various environmental or soil amendment applications.

Figure 4a depicts a graph of zeta potential versus pH for two washed biochar samples, illustrating how their surface charge varies with pH levels. This variation is attributed to factors such as pyrolysis temperature and the aging process.[9] The isoelectric points (pI) for **PScw-1** and **PScw-2** are identified at

pH 2.3 and 6.4, which are the same for both. The existence of two pIs implies the biochar surface has distinct pH values where the net surface charge is neutral, indicating a heterogeneous nature with diverse functional groups. This characteristic, supported by titration data showing both acidic and basic surface groups, influences the biochar's environmental interactions, affecting its adsorption efficiency and contaminant removal capabilities. As shown in Figure 4b, the adsorption of cobalt(II) and nickel(II) ions slightly changed the net surface charge of the **PScw-2** sample. In the case of Co(II) sorption, even the shape of the electrokinetic curve was altered (for a detailed explanation refer to the Adsorption Properties section). A similar phenomenon was observed for the **PScw-1** sample (Figure S3). The changes of the net surface charge and the shape of the electrokinetic dependencies of the sample after adsorption of Co(II) and Ni(II) can denote the adsorption mechanism of the selected metal ions mainly consisting of complexation with positively charged surface groups since the lower value of pI = 2.3 remained unchanged as for bare **PScw-1**.

The infrared spectroscopic analysis (Figure S4) of biochar specimens **PScw-1** and **PScw-2** reveals diverse absorption bands indicative of assorted functional groups. The spectral peaks situated at approximately 3413 and 3617 cm^{-1} are attributed to the stretching vibrations of the O−H bonds, denoting the existence of free hydroxyl groups and hydrogen-bonded hydroxyl entities, respectively. The peak at 3020 cm^{-1} is representative of the =C−H stretching vibrations found in alkenes or aromatic compounds. Absorption bands manifesting at 2920 and 2850 cm^{-1} are characteristic of C−H stretching vibrations within aliphatic hydrocarbons. Additionally, a notable peak at 1694 cm^{-1} is consistent with the stretching vibrations of C=O bonds, suggesting the presence of carbonyl functionalities.[34] The bands located near 1587 and 1430 cm^{-1} are indicative of NH_2 bending vibrations and C−O−H bending motions, respectively, while absorption features around 1378 cm^{-1} denote −CH_2 and −CH_3 deformation bending. Complex vibrational modes observed at 1245 and 1248 cm^{-1} combine attributes of phosphonate, C−N
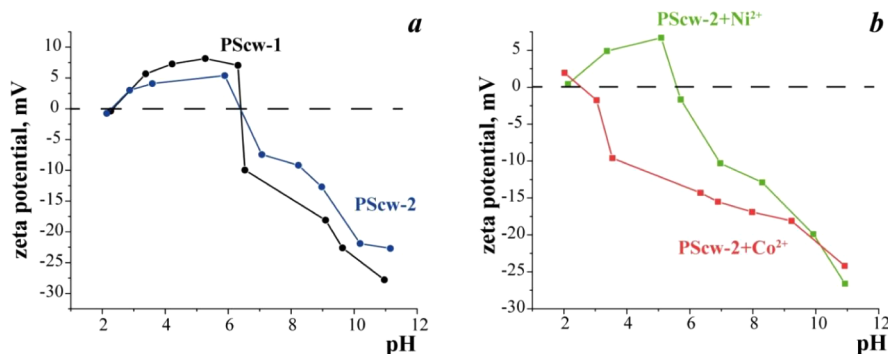
Figure 4. Changes in electrokinetic potential values depending on pH for washed biochar samples (a) and loaded **PScw-2** samples (b).

stretching, and O−C stretching from carboxylic groups.[35] The peak at 1169 cm^{-1} is suggestive of Si−O−Si vibrations characteristic of silicon dioxide, while those at 874 and 810 cm^{-1} are associated with C−H bending and ring puckering in aromatic structures as well as for carbonate. Finally, the absorption peak discerned at 745 cm^{-1} could be indicative of out-of-plane C−H bending in aromatic frameworks, high-lighting the intricate chemical composition and diverse reactive sites within the biochar structure.

Adsorption Properties of Synthesized Biochars toward Ni(II) and Co(II) Ions. Having acidic and basic groups on their surface, such biochar beads could be used as adsorbents; therefore, the adsorption of nickel and cobalt ions from aqueous solutions was studied. In general, adsorption of nickel and cobalt onto specific adsorbents with chelate groups presents a challenging task.[49] Thus, to study the static sorption capacity (SSC) of the samples, experiments were conducted to investigate the dependence of adsorption on the concentration of the initial solution, and the isotherms are depicted in Figure 5.
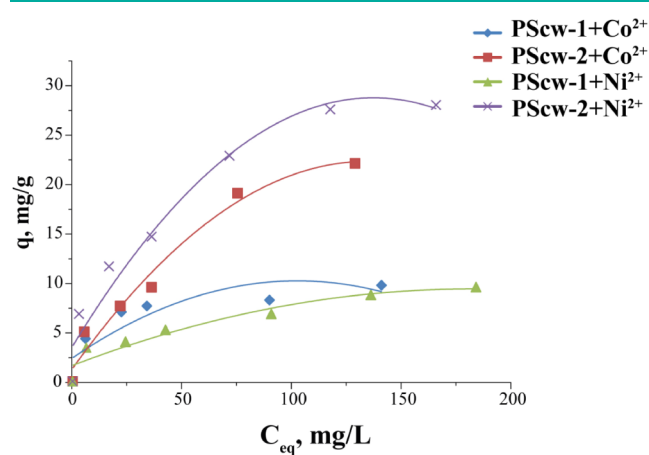

Figure 5. Isotherms of metal ions adsorption for the **PScw-1** and **PScw-2** samples (symbols are experimental points, and lines are trend lines).

The SSC values are listed in Table 3. Given that the raw materials for the samples were the same, and only the pyrolysis temperature varied, which influenced the value of the specific surface area and the number and quality of functional groups, we can deduce that the porous **PScw-2** sample exhibits the best sorption capacity. Despite having a lower specific surface area, it contains more functional groups. **PScw-2** shows a higher adsorption capacity for both ions compared to **PScw-1**, indicating that the properties of **PScw-2** favor the adsorption process. The curves suggest that the adsorption capacity reaches a plateau at higher concentrations, typical of a

saturation effect where the available adsorption sites of biochar become fully occupied. The data in Table 3 suggest that the adsorption process is accurately described by both the Langmuir equation, indicating chemisorption, and the Freundlich equation, indicating the presence of various adsorption sites.

After the adsorption of metal cations, the pH changes are not significant, with the pH decreasing from 6.20 to 6.06 for Ni(II) and from 6.00 to 5.95 for Co(II). This may indicate a slight interaction with acidic adsorption centers, releasing protons or the formation of neutralized compounds that hardly affect the pH change.

The EDX spectra in Figure S5 and the mapping of elements also provide evidence of the adsorption of nickel and cobalt ions. Additionally, the mapping reveals the presence of calcium, which aligns with the X-ray data.

The changes in surface charge after adsorption and the potential mechanism can be inferred by analyzing the data on changes in the electrokinetic potential of suspensions with Ni^{2+} and Co^{2+} ions adsorbed (Figure 4b). In both cases, the zeta potential decreases with increasing pH, and the presence of metal ions seems to shift the zeta potential toward a more negative range compared to the pure **PScw-2** sample. Thus, the isoelectric point (pI) changes to 2.6 with cobalt(II) adsorption, and to 2.1 and 5.6 with nickel(II) adsorption. In the case of Co^{2+} adsorption, this indicates that complexes or nonionic compounds are formed with positive groups on the surface, such as amino groups, leaving only acidic groups on the surface. In the case of Ni^{2+}, adsorption involves both acidic and basic groups, which essentially does not alter the shape of the zeta-potential curve; it merely shifts the equivalence points to the acidic pH region. This suggests that the metal ions influence the surface charge of the particles, potentially through the formation of complexes on the surface. Overall, these changes in zeta potential illustrate how the surface charge of particles in aqueous solutions can vary depending on the pH of the environment and the presence of certain metal ions, which is important for understanding colloidal stability and interactions in solutions.

The nature of the complexes formed on the biochar's surface, loaded with Ni^{2+}, was studied using diffuse reflectance electronic spectra (DRES) (Figure 6a). Peaks at 430, 565, and 680 nm suggest the formation of nickel complexes, likely octahedral[50] or tetrahedral,[51] influenced by the biochar's surface moieties (amino, carboxylic, phenolic, phosphates, carbonates). These structures align with nickel(II) complex geometries. Further detailed spectroscopic analysis is needed to precisely identify the complexes and ligands involved. The absorption at 430 nm indicates ligand-to-metal charge transfer, while the 565 nm band may represent a Ni(II) complex with oxalate and amino groups. At the same time, the reflectance

Table 3. Parameters of Ni(II) and Co(II) Ion Sorption by the Biochar Adsorbents within the Coordinates of the Langmuir and Freundlich Equations

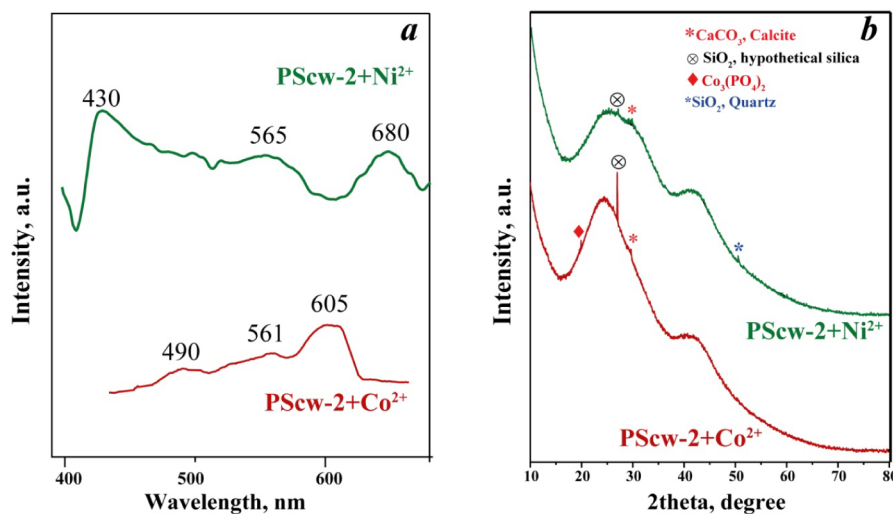| sample	cation	SSC, mg/g	Langmuir equation $C_{eq}/q = 1/(K_L \cdot A_{max}) + (1/A_{max}) \cdot C_{eq}$			Freundlich equation $\ln q = \ln K_F + (1/n) \cdot \ln C_{eq}$		
			A_{max}, mg/g	K_L, L/mg	R^2	K_F, mg/g	$1/n$	R^2
PScw-1	Ni(II)	9.5	3.11	0.628	0.924	27.869	0.09	0.947
	Co(II)	9.7	10.03	0.093	0.986	3.058	0.24	0.903
PScw-2	Ni(II)	27.9	32.29	0.037	0.964	4.341	0.37	0.974
	Co(II)	22.2	30.41	0.019	0.811	1.018	0.65	0.945

Figure 6. DRES (a) and XRD patterns (b) for the biochar sample loaded Ni(II) and Co(II) ions.

spectra of aqua-amino complexes of nickel(II) are characterized by the band at 680 nm.

The diffuse reflectance spectrum of biochar with Co^{2+} shows peaks at 490, 561, and 605 nm, indicating the formation of cobalt complexes with surface functional groups. The peaks may indicate both tetrahedral and octahedral geometries.[51−53] The nature and geometry of these complexes, influenced by the biochar's surface groups, necessitate further analysis through XRD and XPS to determine detailed electronic structures and ligand types involved.

Figure 6b shows two XRD patterns for samples of biochar that have adsorbed Ni(II) and Co(II) ions. The XRD pattern for **PScw-2 + Ni²** is shown in green and features several sharp peaks, indicating the presence of crystalline phases $CaCO_3$ (calcite), SiO_2 (hypothetical silica), and SiO_2 quartz.[54] The XRD pattern for the biochar with adsorbed cobalt ions is shown in red, and compared to the nickel ion-adsorbed biochar has a peak corresponding to $Co_3(PO_4)_2$.[55]

The presence of these symbols indicates the identified crystalline materials within each sample. The marked peaks for calcite, silica, and cobalt phosphate suggest that these materials are present in the structure of the biochar or have been formed during the adsorption process.

To study the chemical composition of bare biochar and that treated with selected metals, X-ray photoelectron spectroscopy (XPS) analysis was conducted, and the results are compiled in Table 4. The survey scan spectrum of bare biochar **PScw-2** revealed the presence of C, O, N, P, and Ca elements. The XPS spectra of the treated samples indicated the presence of Co and Ni, as expected. Detailed analysis of the Co2p and Ni2p spectra suggests that cobalt likely exists in the form of phosphate,[56] while nickel is in the form of nickel(II) hydroxide.[57] Consequently, two principal peaks at 781.39 and 797.10 eV (Δ = 15.7 eV), along with two satellite peaks at 785.26 and 801.80 eV, evidently indicate the formation of $Co_3(PO_4)_2$ in the biochar sample after treatment with a cobalt precursor. This observation is further confirmed by corresponding shifts in binding energies observed in the P2p spectra and inorganic O1s, attributable to changes in the environment surrounding these entities in the biochar sample. The peaks in the Ni2p spectrum, particularly the two main ones at 855.78 and 873.20 eV (Δ = 17.4 eV), were ascribed to nickel(II) hydroxide.

Table 4. Overview of XPS Analysis of Studied Samples

element	binding energy, eV		
	PScw-2	**PScw-2 + Co(II)**	**PScw-2 + Ni(II)**
C1s	284.42 graphite C−C	284.60 graphite C−C	284.36 graphite C−C
	285.95 (C−N, C−O−C)	286.26 (C−N, C−O−C)	285.78 (C−N, C−O−C)
	288.06 O−C=O	288.36 O−C= O	288.16 O−C=O
	290.08 C=O, carbonate	290.34 C=O, carbonate	290.47 C=O, carbonate
O1s	531.37 organic	531.33 organic	531.23 organic
	533.20 inorganic	533.09 inorganic	532.97 inorganic
N1s	399.88 −NH₂, −NH−	399.95 −NH₂, −NH−	399.81 −NH₂, −NH−
P2p	133.26 phosphate	133.34 phosphate	133.25 phosphate
	134.16 phosphate	134.32 phosphate	134.15 phosphate
Ca2p	347.34 CaCO₃	347.56 CaCO₃	347.34 CaCO₃
	350.93 CaCO₃	351.10 CaCO₃	350.94 CaCO₃
other elements		Si2p 102.47 organic	
		Co2p 781.39 Co₃(PO₄)₂	Ni2p 855.78 Ni(OH)₂
		Co2p 785.26 satellite	Ni2p 857.62 satellite
		Co2p 797.10 Co₃(PO₄)₂	Ni2p 873.20 Ni(OH)₂
		Co2p 801.80 satellite	Ni2p 880.10 satellite

The N/C ratio of studied samples demonstrated the increase of N/C is a sample line: bare biochar (0.012) < biochar +Ni(II) (0.018) < biochar+Co(II) (0.024). This fact determines the higher basicity of biochar+Co(II) surface and, therefore, higher affinity toward carbamazepine molecule, which is known to possess a neutral character. Meanwhile, biochar+Co(II) has the highest O/C ratio −0.263, whereas O/C ratios of bare biochar and biochar+Ni(II) were equal to 0.207. The high O/C ratio promotes more intensive production of radicals on the photocatalyst surface, which attack carbamazepine molecules and destroy them.

Thus, the chemisorption of metal cations occurs on the surface of this biochar and in the functional surface groups. Moreover, after adsorption, the **PScw-2** samples contain insoluble calcium carbonate and silicon dioxide. However,

DRES, XRD, and XPS indicated which specific insoluble compounds were formed after adsorption, namely, cobalt phosphate and nickel hydroxide. Such adsorption could be called stagnant, and the regeneration of the sorbent cannot be carried out without using acid, but it turns out that these compounds have interesting properties. For example, cobalt phosphate is used as a photocatalyst,[58] easily producing free radicals, and nickel hydroxide, as indicated by X-ray, can be an electrocatalyst.[47] Therefore, these studies were continued by testing these materials in photocatalysis.

Adsorption of Carbamazepine. It is known that biochar can serve as an adsorbent for removing inorganic and organic pollutants from water due to the presence of functional groups and a high specific surface area. Therefore, before studying photocatalysis, which involves the establishment of equilibrium or adsorption phases, we decided to investigate the sorption properties of the obtained biochar samples (Table S4, Figure S9). Due to the low solubility of carbamazepine in water, the initial solution was consistent over time. Data indicates that carbamazepine is best adsorbed by the sample with the highest number of functional groups **PScw-2**. As can be seen, the adsorption capacities were increased for samples loaded with cobalt and nickel, which confirms the successful functionalization of the biochar with selected metals. Lesser adsorption for sample **PScw-1**, which has a more developed specific surface area, also suggests the likelihood of a chemical interaction. After 5 adsorption cycles (or, in other words, concentration of carbamazepine on the surface), only the pure sample **PScw-2** still has potential for adsorption; the other samples hardly adsorb carbamazepine anymore. An increase in pH from cycle 1 to 5 during adsorption suggests the leaching of calcium compounds, which is evidenced by a peak at 250 nm in the UV spectra (Figure S9).

Photocatalytic Properties of Bare PScw-2 and Loaded with Cobalt(II) and Nickel(II). The photocatalytic degradation of carbamazepine using metal-loaded biochar derived from pine sawdust was systematically studied. The photodegradation kinetic curves are demonstrated in Figure 7. The stability of carbamazepine ($C = 5 \times 10^{-5}$ M) under UV light was confirmed in a control experiment, exhibiting minimal degradation near 2%. This foundational observation underscores the inert nature of carbamazepine toward photolysis, necessitating catalytic intervention for effective degradation. It should be pointed out that the elimination of carbamazepine in
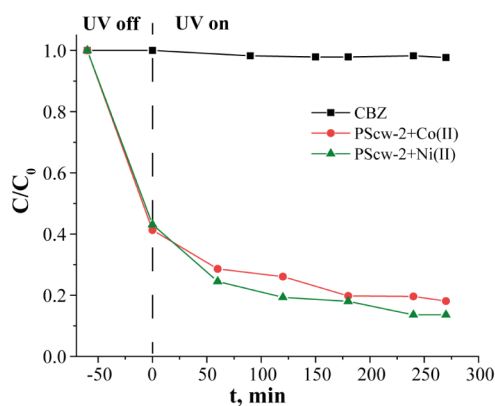

Figure 7. Photocatalytic kinetic curves of carbamazepine degradation (5×10^{-5} M) under UV light in the presence of bare biochar **PScw-2** and loaded with Co(II) and Ni(II).

"UV off" mode was performed by adsorption forces; therefore, the adsorption capacities can be calculated. Thus, for **PScw-2 + Co(II)** was 6.9 mg/g, and **PScw-2 + Ni(II)** was −6.7 mg/g.

Despite the decrease in adsorption capacity, the presence of metals remarkably improves the photocatalytic activity of biochar: from 58.7% of adsorption to 81.9% during photocatalysis for **PScw-2 + Co(II)**, as well as from 56.9% of adsorption to 86.4% during photocatalysis for **PScw-2 + Ni(II)**, respectively in 5.5 h (Figure 8, Figures S9 and S10). The rate constants calculated from the slopes of linear dependences of $\ln(C_o/C) = f(t)$ were: for **PScw-2 + Co(II)** 0.0031 min^{-1} and for **PScw-2 + Ni(II)** 0.0042 min^{-1}. These values are comparable to those from literature,[26] where reaction rate constant was calculated to be 0.0034 min^{-1}. The rate constants not only serve as benchmarks for photocatalytic performance but also pave the way for comparative analyses with existing literature, offering a nuanced understanding of these materials' place within the broader context of photocatalytic research.[58,59]

The stability and reusability of adsorbents and photocatalysts are among the prominent factors in the selection of sustainable and economical water treatment methods. Therefore, the changes in the performance of adsorption and photocatalysis of carbamazepine in 5 cycles were studied (Figures S9 and S14). As shown in Figure 8, the adsorption and photocatalytic removal percentages gradually decreased from cycle to cycle with the lowest values for the fifth cycle. It is very interesting that during the cyclic adsorption, the pH of the final solution became more basic for both materials **PScw-2 + Co(II)** and **PScw-2 + Ni(II)**. Additionally, the small new peak approximately at $\lambda = 250$ nm appears on carbamazepine spectra after three adsorption cycles (Figure S9). This fact can be explained by the release of calcium compounds (probably, calcium carbonate)[60] from the biochar since some of them are still left in the samples after washing (XRD and XPS data). The data from the photocatalytic removal of carbamazepine demonstrated better regeneration abilities and higher performance of the studied samples under UV light (Figure 9). The materials retained satisfactory efficiency even at the third cycle in comparison to data from adsorption. The changes in the pH were also monitored. Thus, for 5 cycles of photocatalysis in the presence of **PScw-2 + Co(II)** the pH remained stable. However, for **PScw-2 + Ni(II)** a slight decrease in pH was observed.

The radical trapping experiments were performed to better understand the processes occurring during light exposure to the studied systems (Figure 9). For this purpose, three scavengers were chosen: EDTA+2Na for trapping positively charged holes h$^+$, sodium sulfate as an electron scavenger, and isopropanol for capturing hydroxyl radicals ●OH. The concentration of each substance was 2 mM.

Thus, EDTA+2Na is a known hole scavenger with retarded charge recombination properties. The addition of 2 mM of EDTA+2Na into the studied system influenced the kinetics of the removal of CBZ, especially under the "UV on" mode (Figure S11). Indeed, the comparison of first-order model rate constants did not result in reduced reduction: k(**PScw-2 + Co(II)**) = 0.0031 min^{-1}, k(**PScw-2 + Co(II) + EDTA**) = 0.0029 min^{-1}; and demonstrated the significant reduction in the removal rates in the presence of EDTA: k(**PScw-2 + Ni(II)**) = 0.0042 min^{-1}, k(**PScw-2 + Ni(II) + EDTA**) = 0.0011 min^{-1}. This discovery helps to suggest that holes play a crucial role in the elimination of CBZ for the **PScw-2 + Ni(II)**

Adsorption

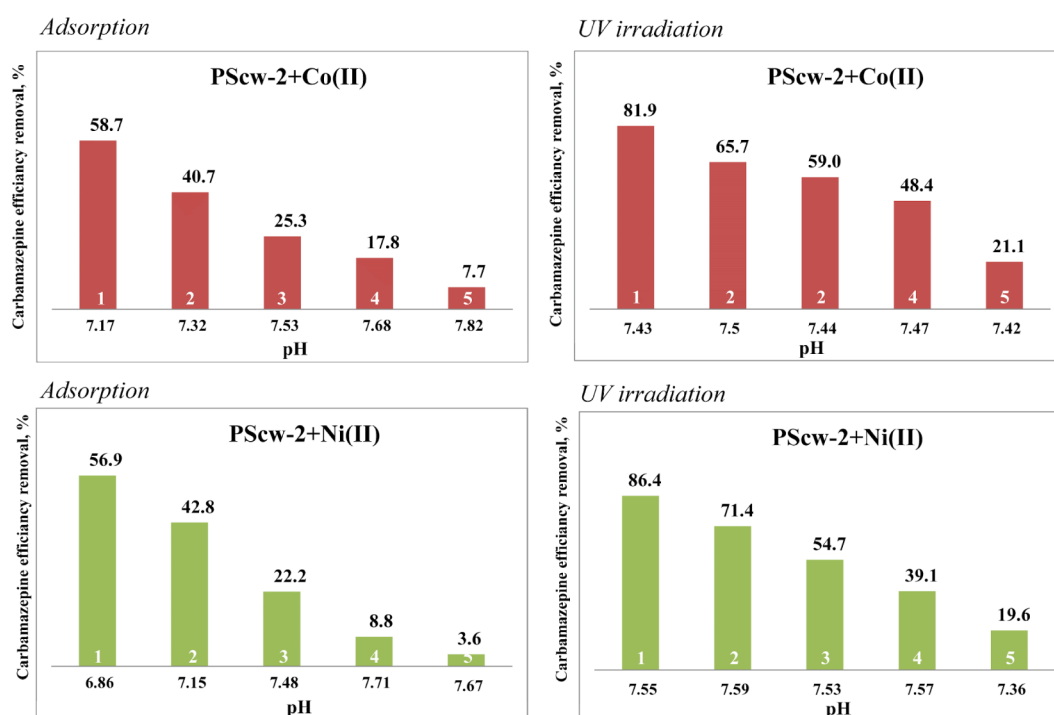*UV irradiation*

Adsorption

UV irradiation

Figure 8. Comparison of data on the efficiency of carbamazepine removal in 5 cycles of adsorption and photocatalysis (under other identical conditions) for the samples **PScw-2 + Co(II)** and **PScw-2 + Ni(II)**.

sample. Another noted scavenger is sodium sulfate, which is an electron scavenger. The presence of sodium sulfate also affected the rate of removal under the "UV on" regime (Figure 9, Figure S12). Thus, the rate constant of the system **PScw-2 + Co(II) + Na₂SO₄** decreased and was calculated to be 0.0021 min⁻¹. However, surprisingly for us, the interfering effect of sodium sulfate on carbamazepine uptake with **PScw-2 + Ni(II)** was also observed (k(**PScw-2 + Ni(II) + Na₂SO₄**) = 0.0032 min⁻¹), though it was less pronounced than with EDTA+2Na. Similar observations were done for the same systems but with isopropanol as a hydroxyl radical trap (Figure 9, Figure S13). A 2-fold decrease in elimination rate was observed for a system with Co(II) (k = 0.0016 min⁻¹), whereas the biochar loaded with Ni(II) also showed a nearly 2-fold decreased value of k = 0.0024 min⁻¹. To sum up, the studied materials exhibited different mechanisms of carbamazepine removal. Hence, the effect of electrons and hydroxyl radicals was predominant during the light exposure to the **PScw-2 + Co(II) + CBZ** system, while electron/hole recombinations and hydroxyl radicals were responsible for the elimination of carbamazepine using **PScw-2 + Ni(II)**.

Other interesting observations were made based on the changes in UV−vis spectra of carbamazepine during the performed tests (Figure S10). A recorded UV−vis spectrum of CBZ possesses several peaks at 210, 240, and 285 nm. The shoulder at 240 nm corresponds to $\pi-\pi$ transitions in the aromatic ring system. These transitions involve the movement of electrons from the highest occupied molecular orbital (HOMO) to the lowest unoccupied molecular orbital (LUMO). On the spectra recorded after light exposure in the presence of **PScw-2 + Co(II)** and **PScw-2 + Ni(II)**, the intensity of this shoulder was strongly reduced and even absent on some spectra. Additionally, the intensity of the main peak at 285 nm also reduces during the measurements without any

shift in the wavelength. The occurrence of open-ring products of carbamazepine degradation was described by Chen.[22]

This study also paves the way for further inquiries into the mechanism of photodegradation facilitated by metal-loaded biochars. The involvement of specific reactive oxygen species, the role of biochar's surface properties, and the impact of metal loading on these parameters emerge as pivotal areas for future research. Additionally, exploring the scalability of this approach and its environmental implications, especially in terms of practical water treatment applications, could significantly contribute to the field of environmental remediation.

In conclusion, the metal-loaded biochars exhibit promising photocatalytic activity toward the degradation of carbamazepine, highlighting their potential as efficient and environmentally benign photocatalysts. Further research into the underlying mechanisms, environmental impact, and scalability of this approach will be crucial in harnessing the full potential of these materials for water purification and environmental protection efforts.

■ CONCLUSIONS

Our research demonstrates the effective transformation of pine sawdust waste into a valuable biochar that serves multiple environmental remediation purposes. By utilizing plant residues from *Pinus sylvestris*, we have created sustainable biochar materials with enhanced adsorptive properties for the effective removal of cobalt(II) and nickel(II) ions from aqueous solutions. The biochar samples displayed intricate morphological features, comprising both fibrous structures and particulate clusters, associated with a substantial degree of porosity and surface irregularities. The prepared biochars effectively adsorbed Co(II) and Ni(II), achieving equilibrium capacities of 0.38 and 0.48 mmol per 1 g of biochar, respectively, synthesized under a gradual temperature increase mode. Cobalt phosphate and nickel hydroxide formed on the
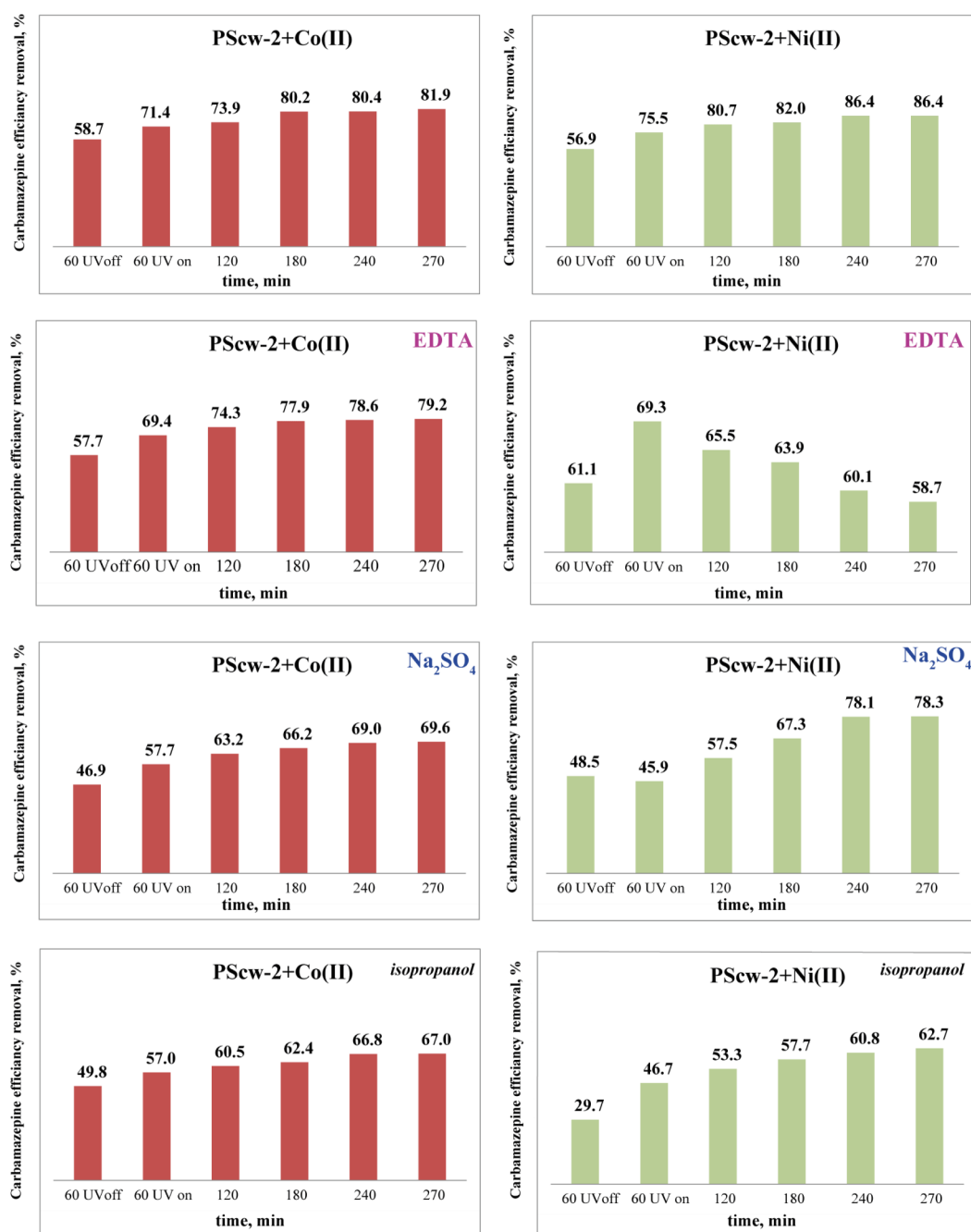
Figure 9. Effect of adding different scavengers on the photocatalytic degradation of carbamazepine using samples **PScw-2 + Co(II)** and **PScw-2 + Ni(II)**.

biochar surface are known for their photocatalytic applications. Therefore, the loaded biochars were utilized to reduce the concentration of carbamazepine under UV light exposure, achieving a removal efficiency of over 80%. The elimination followed a first-order kinetic model with rate constants of $0.0031-0.0042$ min^{-1}, comparable to those described in the available literature. The complex physicochemical interactions were found to be responsible for carbamazepine removal. Experiments with radical traps helped to better understand the mechanism of the carbamazepine concentration decrease, revealing that electron/hole recombination and hydroxyl radicals were predominant during light exposure to cobalt-laden biochar in the presence of carbamazepine, whereas hydroxyl radicals were primarily responsible for the removal

using nickel-loaded biochar. The reusability of spent loaded biochars was also tested under 5 cycles. The first 2 cycles showed satisfactory carbamazepine adsorptive removal, with efficacy declining in subsequent cycles. Under UV light, the efficiency remained high (over 50%) even in the third cycle, with a gradual decrease in the remaining cycles. This confirms the beneficial use of UV light in carbamazepine elimination. Additionally, the disappearance of the shoulder in UV−vis spectra of carbamazepine exposed to UV light could indicate certain chemical transformations of carbamazepine molecules, mainly the destruction of the aromatic ring system, forming open-ring structures. These observations can be encouraging for further in-depth studies of the processes that have occurred.

In summary, the developed biochars not only exhibit excellent adsorption capacity for heavy metal ions but also demonstrate significant potential in degrading persistent pharmaceutical contaminants under UV irradiation, offering a dual-function solution to water pollution. Finally, the research emphasizes the importance of developing cost-effective, sustainable, and efficient methods for waste treatment and environmental protection. It encourages the repurposing of biomass waste into valuable materials for environmental remediation, aligning with global sustainability goals.

■ ASSOCIATED CONTENT

Ⓢ Supporting Information

The Supporting Information is available free of charge at https://pubs.acs.org/doi/10.1021/acsestwater.4c00241.

Additional experimental details, materials, and methods; additional results related to the effect of pyrolysis temperature on the texture and structure of the obtained materials; TGA curves for the initial carbonized samples and its analysis; XRD patterns of as-prepared and washed biochars and its analysis; changes in electro-kinetic potential values depending on pH for Co(II) and Ni(II) loaded **PScw-1** samples; IR spectra of the **PScw-1** and **PScw-2** samples; EDX spectra and element maps for **PScw-2** loaded Ni(II) and Co(II); survey XPS spectra of the **PScw-2**, **PScw-2 + Ni(II)**, **PScw-2 + Co(II)** samples, and XPS spectra of N 1s, Ca 2p, P 2p, Si 2p, O 1s, C 1s, Ni 2p, and Co 2p orbitals and their XPS data; table data with the efficiency of carbamazepine extraction and pH changes during 5 cycles of adsorption on all samples ($m = 0.05$g, $V = 50$ mL, $t = 5.5$h, $C_{CMZ} = 11.8$ mg/L); UV−vis spectra of carbamazepine solutions after adsorption in 5 cycles for all biochar samples; UV−vis spectra of carbamazepine solutions during UV treatment with **PScw-2 + Co(II)** and **PScw-2 + Ni(II)** biochar samples, as well as during EDTA-2Na, Na$_2$SO$_4$, isopropanol trapping agent experiments; UV−vis spectra of carbamazepine solutions during UV treatment with **PScw-2 + Co(II)** and **PScw-2 + Ni(II)** biochar samples in 5 cycles of experiments (PDF)

■ AUTHOR INFORMATION

Corresponding Authors

Halyna Bodnár Yankovych − *Department of Physical and Physico-Chemical Methods of Mineral Processing, Institute of Geotechnics, Košice, SAS 04001, Slovak Republic;* ⓞ orcid.org/0000-0003-4332-5924; Email: yankovych@saske.sk

Inna V. Melnyk − *Department of Chemisorption and Hybrid Materials, Chuiko Institute of Surface Chemistry, National Academy of Sciences of Ukraine, Kyiv 03164, Ukraine; Department of Physical and Physico-Chemical Methods of Mineral Processing, Institute of Geotechnics, Košice, SAS 04001, Slovak Republic;* ⓞ orcid.org/0000-0002-2559-5771; Email: melnyk@saske.sk

Authors

Anna Yukhymchuk − *Natural Faculty, Department of Chemistry, Dragomanov Ukrainian State University, Kyiv 01601, Ukraine*

Daria Zhukova − *Natural Faculty, Department of Chemistry, Dragomanov Ukrainian State University, Kyiv 01601, Ukraine*

Nataliia Prybora − *Natural Faculty, Department of Chemistry, Dragomanov Ukrainian State University, Kyiv 01601, Ukraine*

Nataliya Stolyarchuk − *Department of Chemisorption and Hybrid Materials, Chuiko Institute of Surface Chemistry, National Academy of Sciences of Ukraine, Kyiv 03164, Ukraine*

Oleksandr Bondarchuk − *INL - International Iberian Nanotechnology Laboratory, Braga 4715-330, Portugal; SPIN-Lab Centre for Microscopic Research on Matter, University of Silesia in Katowice, Chorzów 41-500, Poland; Institute of Chemistry, University of Silesia in Katowice, Katowice 40-006, Poland;* ⓞ orcid.org/0000-0001-7380-8930

Complete contact information is available at:
https://pubs.acs.org/10.1021/acsestwater.4c00241

Author Contributions

CRediT: **Anna Yukhymchuk** formal analysis, investigation, methodology, writing-original draft; **Daria Zhukova** formal analysis, investigation, methodology; **Nataliia Prybora** data curation, formal analysis, investigation, methodology, writing-original draft, supervision; **Nataliia Stolyarchuk** formal analysis, investigation; **Oleksandr Bondarchuk** formal analysis, investigation; **Halyna Bodnár Yankovych** conceptualization, data curation, investigation, methodology, writing-original draft; **Inna V. Melnyk** conceptualization, project administration, resources, supervision, writing-review & editing.

Notes

The authors declare no competing financial interest.

■ ACKNOWLEDGMENTS

■ REFERENCES

(1) Eurostat Statistics Explained. https://www.ec.europa.eu/eurostat/statistics-explained/index.php?title=Waste_statistics (accessed 06 august 2024).

(2) Carmo, F. F.; Lanchotti, A. O.; Kamino, L. H. Y. Mining waste challenges: Environmental risks of gigatons of mud, dust and sediment in megadiverse regions in Brazil. *Sustainability* **2020**, *12*, 8466.

(3) Vieira, R. F.; Lopes, D.; Baptista, I.; Figueiredo, S.; Domingues, V.; Vaz, J.; Varela, H.; Jorge, R.; Freitas, O. M.; Delerue-Matos, C.; Brebbia, C. A. Biofiltration using natural materials from Portuguese woods for odour removal in a municipal waste management plant. In *Sustainable Development*. WIT Transactions on the Built Environment, 2015, 82, 717.

(4) Yaman, S. Pyrolysis Of Biomass To Produce Fuels And Chemical Feedstocks. *Energy Convers. Manag.* **2004**, *45* (5), 651−671.

(5) Mishra, S.; Upadhyay, R. K. Review on biomass gasification: Gasifiers, gasifying mediums, and operational parameters. *Mater. Sci. Energy Technol.* **2021**, *4*, 329−340.

(6) Bentley, M. J.; Summers, R. S. Ash pretreatment of pine and biosolids produces biochars with enhanced capacity for organic micropollutant removal from surface water, wastewater, and stormwater. *Environ. Sci.: Water Res. Technol.* **2020**, *6*, 635−644.

(7) Musapatika, E. T.; Singh, R.; Moodley, K.; Nzila, C.; Onyango, M.; Ochieng, A. Cobalt removal from wastewater using pine sawdust. *Afr. J. Biotechnol.* **2012**, *11* (39), 9407−9415.

(8) Rashad, E.; Saleh, H. N.; Eltaweil, A. S.; Saleh, M. E.; Sillanpaa, M.; Mostafa, A. R. Pinewood sawdust biochar as an effective biosorbent for PAHs removal from wastewater. *Biomass Convers. Biorefin.* **2023**, *13*, 13443−13459.

(9) Liu, L.; Deng, G.; Shi, X. Adsorption characteristics and mechanism of p-nitrophenol by pine sawdust biochar samples produced at different pyrolysis temperatures. *Sci. Rep.* **2020**, *10*, 5149.

(10) Anastopoulos, I.; Katsouromalli, A.; Pashalidis, I. Oxidized biochar obtained from pine needles as a novel adsorbent to remove caffeine from aqueous solutions. *J. Mol. Liq.* **2020**, *304*, 112661.

(11) Kim, J.; Bak, G. H.; Yoo, D. Y.; Lee, Y. I.; Lee, Y. G.; Chon, K. Functionalization of pine sawdust biochars with Mg/Al layered double hydroxides to enhance adsorption capacity of synthetic azo dyes: Adsorption mechanisms and reusability. *Heliyon* **2023**, *9* (3), No. e14142.

(12) Bhatnagar, A.; Sillanpää, M. Utilization of agro-industrial and municipal waste materials as potential adsorbents for water treatment—A review. *J. Chem. Eng.* **2010**, *157* (2−3), 277−296.

(13) Ortúzar, M.; Esterhuizen, M.; Olicón-Hernández, D. R.; González-López, J.; Aranda, E. Pharmaceutical pollution in aquatic environments: A concise review of environmental impacts and bioremediation systems. *Front. Microbiol.* **2022**, *13*, 869332.

(14) Wilkinson, J. L.; Boxall, A. B. A.; Kolpin, D. W.; Leung, K. M. Y.; Lai, R. W. S.; Galbán-Malagón, C.; Adell, A. D.; Mondon, J.; Metian, M.; Marchant, R. A.; et al. Pharmaceutical pollution of the world's rivers. *Proc. Natl. Acad. Sci. U. S. A.* **2022**, *119*, No. e2113947119.

(15) Speed, D.; Dickson, S.; Cairns, E.; Kim, N. Analysis of six anticonvulsant drugs using solid-phase extraction, deuterated internal standards, and gas chromatography-mass spectrometry. *J. Anal. Toxicol.* **2000**, *24*, 685−690.

(16) Clara, M.; Strenn, B.; Kreuzinger, N. Carbamazepine as a possible anthropogenic marker in the aquatic environment: Investigations on the behaviour of Carbamazepine in wastewater treatment and during groundwater infiltration. *Water Res.* **2004**, *38* (4), 947−954.

(17) CCME. Scientific criteria document for the development of the Canadian water quality guideline for Carbamazepine. In *Protection of Aquatic Life. Canadian Council of Ministers of the Environment*: CCME Winnipeg, MB, 2018.

(18) *Groundwater quality standards for proposed additional pollutants in the annexes to the Groundwater Directive (2006/118/EC)*:https://health.ec.europa.eu/publications/groundwater-quality-standards-proposed-additional-pollutants-annexes-groundwater-directive-2006118ec_en. 2024.

(19) Öllers, S.; Singer, H. P.; Fässler, P.; Müller, S. R. Simultaneous quantification of neutral and acidic pharmaceuticals and pesticides at the low-ng/l level in surface and wastewater. *J. Chromatogr. A* **2001**, *911*, 225−234.

(20) *Occurrence and seasonal variability of selected pharmaceuticals in southern ontario drinking water supplies*, https://uwspace.uwaterloo.ca/bitstream/handle/10012/2774/MSc_Thesis_JKormos_Final.pdf?sequence=1&isAllowed=y, 2024.

(21) Metcalfe, C. D.; Koenig, B. G.; Bennie, D. T.; Servos, M.; Ternes, T. A.; Hirsch, R. Occurrence of neutral and acidic drugs in the effluents of Canadian sewage treatment plants. *Environ. Toxicol. Chem.* **2003**, *22*, 2872−2880.

(22) Chen, G.; Dong, W.; Wang, H.; Zhao, Z.; Wang, F.; Wang, F.; Nieto-Delgado, C. Carbamazepine degradation by visible-light-driven photocatalyst Ag₃PO₄/GO: Mechanism and pathway. *Environ. Sci. Ecotechnology* **2022**, *9*, 100143.

(23) Batucan, N. P.; Tremblay, L. A.; Northcott, G. L.; Matthaei, C. D. Medicating the environment? A critical review on the risks of carbamazepine, diclofenac and ibuprofen to aquatic organisms. *Environ. Adv.* **2022**, *7*, 100164.

(24) Dhiman, P.; Patial, M.; Kumar, A.; Alam, M.; Naushad, M.; Sharma, G.; Vo, D.-V. N.; Kumar, R. Environmental friendly and robust Mg₀.₅₋ₓCuₓZn₀.₅Fe₂O₄ spinel nanoparticles for visible light driven degradation of Carbamazepine: Band shift driven by dopants. *Mater. Lett.* **2021**, *284*, 129005.

(25) Xu, J.; Li, L.; Guo, C.; Zhang, Y.; Meng, W. Photocatalytic degradation of carbamazepine by tailored BiPO₄: efficiency, intermediates and pathway. *Appl. Catal., B* **2013**, *130*, 285−292.

(26) Kane, A.; Chafiq, L.; Dalhatou, S.; Bonnet, P.; Nasr, M.; Gaillard, N.; Dangwang Dikdim, J. M. D.; Monier, G.; Assadi, A. A.; Zeghioud, H. g-C₃N₄/TiO₂ S-scheme heterojunction photocatalyst with enhanced photocatalytic Carbamazepine degradation and mineralization. *J. Photochem. Photobiol., A* **2022**, *430*, 113971.

(27) Gao, X.; Guo, Q.; Tang, G.; Peng, W.; Luo, Y.; He, D. Effects of inorganic ions on the photocatalytic degradation of carbamazepine. *J. Water Reuse Desalin* **2019**, *9* (3), 301−309.

(28) Meribout, R.; Zuo, Y.; Khodja, A. A.; Piram, A.; Lebarillier, S.; Cheng, J.; Wang, C.; Wong-Wah-Chung, P. Photocatalytic degradation of antiepileptic drug carbamazepine with bismuth oxychlorides (BiOCl and BiOCl/AgCl composite) in water: Efficiency evaluation and elucidation degradation pathways. *J. Photochem. Photobiol. A: Chem.* **2016**, *328*, 105−113.

(29) Li, L.; Zhang, Y.; Yang, S.; Zhang, S.; Xu, Q.; Chen, P.; Du, Y.; Xing, Y. Cobalt-loaded cherry core biochar composite as an effective heterogeneous persulfate catalyst for bisphenol A degradation. *RSC Adv.* **2022**, *12*, 7284−7294.

(30) Rubén, R.; Abdelkader-Fernández, V. K.; Matos, R.; Peixoto, A. F.; Fernandes, D. M. Metal-supported biochar catalysts for sustainable biorefinery, electrocatalysis, and energy storage applications: A review. *Catalysts* **2022**, *12* (2), 207.

(31) Cao, T.; Cui, H.; Zhang, Q.; Cui, C. Facile synthesis of Co(II)-BiOCl@biochar nanosheets for photocatalytic degradation of p-nitrophenol under vacuum ultraviolet (VUV) irradiation. *Appl. Surf. Sci.* **2021**, *559*, 149938.

(32) Murugesan, A.; Loganathan, M.; Kumar, P. S.; Vo, D.-V. N. Cobalt and nickel oxides supported activated carbon as an effective photocatalysts for the degradation Methylene Blue dye from aquatic environment. *Sustain Chem. Pharm.* **2021**, *21*, 100406.

(33) Wei, S.; Zhu, M.; Fan, X.; Song, J.; Peng, P.; Li, K.; Jia, W.; Song, H. Influence of pyrolysis temperature and feedstock on carbon fractions of biochar produced from pyrolysis of rice straw, pine wood, pig manure and sewage sludge. *Chemosphere* **2019**, *218*, 624−631.

(34) Korus, A.; Szlęk, A.; Samson, A. Physicochemical properties of biochars prepared from raw and acetone-extracted pine wood. *Fuel Process. Technol.* **2019**, *185*, 106−116.

(35) Yu, S.; Wu, L.; Ni, J.; Zhang, H.; Wei, R.; Chen, W. The chemical compositions and carbon structures of pine sawdust- and wheat straw-derived biochars produced in air-limitation, carbon dioxide, and nitrogen atmospheres, and their variation with charring temperature. *Fuel* **2022**, *315*, 122852.

(36) Boehm, H. P. Surface oxides on carbon and their analysis: A critical assessment. *Carbon* **2002**, *40*, 145−149.

(37) Yankovych, H.; Bodnár, G.; Elsaesser, M. S.; Fizer, M.; Storozhuk, L.; Kolev, H.; Melnyk, I.; Václavíková, M. Carbon composites for rapid and effective photodegradation of 4-halogenophenols: Characterization, removal performance, and computational studies. *J. Photochem. Photobiol. A Chem.* **2023**, *441*, 114753.

(38) Vijayaraghavan, K.; Balasubramanian, R. Application of pinewood waste-derived biochar for the removal of nitrate and phosphate from single and binary solutions. *Chemosphere* **2021**, *278*, 130361.

(39) Kim, K. H.; Kim, J. Y.; Cho, T. S.; Choi, W. J. Influence of pyrolysis temperature on physicochemical properties of biochar obtained from the fast pyrolysis of pitch pine (Pinus rigida). *Bioresour. Technol.* **2012**, *118*, 158−162.

(40) Jain, M.; Garg, V. K.; Kadirvelu, K.; Sillanpaa, M. Adsorption of heavy metals from multi-metal aqueous solution by sunflower plant biomass-based carbons. *Int. J. Environ. Sci. Technol.* **2016**, *13*, 493−500.

(41) Chen, T.; Zhang, Y.; Wang, H.; Lu, W.; Zhou, Z.; Zhang, Y.; Ren, L. Influence of pyrolysis temperature on characteristics and heavy metal adsorptive performance of biochar derived from municipal sewage sludge. *Bioresour. Technol.* **2014**, *164*, 47−54.

(42) Yankovych, H.; Novoseltseva, V.; Kovalenko, O.; Behunova, D. M.; Kanuchova, M.; Vaclavikova, M.; Melnyk, I. New perception of Zn (II) and Mn (II) removal mechanism on sustainable sunflower biochar from alkaline batteries contaminated water. *J. Environ. Manag.* **2021**, *292*, 112757.

(43) Vaičiukynienė, D.; Alaburdaitė, R.; Nizevičienė, D.; Tamošaitis, G. Sorption properties of Pb^{2+} ions from water by alkali activated slag/biochar composites. *Biomass Conv. Bioref.* **2024**, 1−3.

(44) Putman, K. J.; Rowles, M. R.; Marks, N. A.; de Tomas, C.; Martin, J. W.; Suarez-Martinez, I. Defining graphenic crystallites in disordered carbon: Moving beyond the platelet model. *Carbon* **2023**, *209*, 117965.

(45) Paris, O.; Zollfrank, C.; Zickler, G. A. Decomposition and carbonisation of wood biopolymers—a microstructural study of softwood pyrolysis. *Carbon* **2005**, *43* (1), 53−66.

(46) Guo, Z.; Chen, R.; Yang, R.; Yang, F.; Chen, J.; Li, Y.; Zhou, J.; Xu, J. Synthesis of amino-functionalized biochar/spinel ferrite magnetic composites for low-cost and efficient elimination of Ni (II) from wastewater. *Sci. Total Environ.* **2020**, *722*, 137822.

(47) Novoseltseva, V.; Yankovych, H.; Kovalenko, O.; Vaclavikova, M.; Melnyk, I. Production of high-performance lead(II) ions adsorbents from pea peels waste as a sustainable resource. *Waste Manag. Res.* **2021**, *39*, 584−593.

(48) Tan, Z.; Ye, Z.; Zhang, L.; Huang, Q. Application of the ^{15}N tracer method to study the effect of pyrolysis temperature and atmosphere on the distribution of biochar nitrogen in the biomass−biochar-plant system. *Sci. Total Environ.* **2018**, *622−623*, 79−87.

(49) Deepatana, A.; Valix, M. Comparative adsorption isotherms and modeling of nickel and cobalt citrate complexes onto chelating resins. *Desalination* **2008**, *218*, 334−342.

(50) Song, Y.; Massera, C.; van Albada, G. A.; Manotti Lanfredi, A. M. M.; Reedijk, J. Synthesis, structural characterisation and solvatochromism of a Ni(II) and a Co(II) compound with 2-aminopyrimidine as a ligand. *J. Mol. Struct.* **2005**, *734*, 83−88. ISSN 0022−2860

(51) Sarı, N.; ̧ahin, S.; Öütcü, H.; Dede, Y.; Yalcin, S.; Altundaş, A.; Döanay, K. Ni(II)-tetrahedral complexes: Characterization, antimicrobial properties, theoretical studies and a new family of charge-transfer transitions. *Spectrochim. Acta - A: Mol. Biomol. Spectrosc.* **2013**, *106*, 60−67.

(52) Vakros, J.; Bourikas, K.; Perlepes, S.; Kordulis, C.; Lycourghiotis, A. Adsorption of cobalt ions on the "electrolytic solution/gamma-alumina" interface studied by diffuse reflectance spectroscopy (DRS). *Langmuir* **2004**, *20*, 10542−10550.

(53) Bhuiyan, A. A.; Dossey, R.; Anderson, T. J.; Millett, F.; Durham, B. Synthesis and Characterization of Ruthenium(II) Phenanthroline Complexes Containing Quaternary Amine Substituents. *J. Coord. Chem.* **2008**, *61*, 2009−2016.

(54) Natkaniec-Nowak, L.; Dumańska-Słowik, M.; Gaweł, A.; Łatkiewicz, A.; Kowalczyk-Szpyt, J.; Wolska, A.; Milovská, S.; Luptáková, J.; Ładoń, K. Fire agate from the Deer Creek deposit (Arizona, USA) − new insights into structure and mineralogy. *Mineral. Mag.* **2020**, *84* (2), 343−354.

(55) Shao, Y.; Xiao, X.; Zhu, Y.; Ma, T. Single-crystal cobalt phosphate nanosheets for biomimetic oxygen evolution in neutral electrolytes. *Angew. Chem., Int. Ed.* **2019**, *58*, 14599−14604.

(56) Mao, H.; Zhang, F.; Liu, X.; Qiu, J.; Li, B.; Jin, Z. 2018 Synthesis of cobalt phosphate nanoflakes for high-performance flexible symmetric supercapacitors. *J. Mater. Sci.: Mater. Electron.* **2018**, *29*, 16721−16729.

(57) Li, X.; Patil, K.; Agarwal, A.; Babar, P.; Jang, J. S.; Chen, X.; Yoo, Y. T.; Kim, J. H. Ni $(OH)_2$ coated CoMn-layered double hydroxide nanowires as efficient water oxidation electrocatalysts. *New J. Chem.* **2022**, *46*, 2044−2052.

(58) Jiang, H.; Li, J.; Rao, X.; Zhang, Y. Construction of $Co_3(PO_4)_2$/g-C_3N_4 nanowire composites to boost visible-light-driven photocatalysis. *Energy Adv.* **2023**, *2*, 1419−1428.

(59) Gupta, S.; Patel, P.; Mondal, P. Environmental footprints of the catalytic pyrolysis of pine needles through integration of a nickel-decorated chemically modified biochar catalyst. *ACS Sustainable Chem. Eng.* **2023**, *11*, 5577−5588.

(60) Al Omari, M. M. H.; Rashid, I. S.; Qinna, N. A.; Jaber, A. M.; Badwan, A. A. Chapter Two - Calcium Carbonate. *Profiles Drug Subst., Excipients, Relat. Methodol.* **2016**, *41*, 31−132.